Published in final edited form as:
Chem Biol Interact. 2011 May 30; 191(1-3): 42–47. doi:10.1016/j.cbi.2010.12.015.

Origins of the High Catalytic Activity of Human Alcohol Dehydrogenase 4 Studied with Horse Liver A317C Alcohol Dehydrogenase

Timothy J. Herdendorf[1] and **Bryce V. Plapp**[*]
Department of Biochemistry, The University of Iowa, Iowa City, IA 52242-1109 USA

Abstract

The turnover numbers and other kinetic constants for human alcohol dehydrogenase (ADH) 4 ("stomach" isoenzyme) are substantially larger (10–100-fold) than those for human class I and horse liver alcohol dehydrogenases. Comparison of the primary amino acid sequences (69% identity) and tertiary structures of these enzymes led to the suggestion that residue 317, which makes a hydrogen bond with the nicotinamide amide nitrogen of the coenzyme, may account for these differences. Ala-317 in the class I enzymes is substituted with Cys in human ADH4, and locally different conformations of the peptide backbones could affect coenzyme binding. This hypothesis was tested by making the A317C substitution in horse liver ADH1E and comparisons to the wild-type ADH1E. The steady-state kinetic constants for the oxidation of benzyl alcohol and the reduction of benzaldehyde catalyzed by the A317C enzyme were very similar (up to about 2-fold differences) to those for the wild-type enzyme. Transient kinetics showed that the rate constants for binding of NAD^+ and NADH were also similar. Transient reaction data were fitted to the full ordered bi bi mechanism and showed that the rate constants for hydride transfer decreased by about 2.8-fold with the A317C substitution. The structure of A317C ADH1E complexed with NAD^+ and 2,3,4,5,6-pentafluorobenzyl alcohol at 1.2 Å resolution is essentially identical to the structure of the wild-type enzyme, except near residue 317 where the additional sulfhydryl group displaces a water molecule that is present in the wild-type enzyme. ADH is adaptable and can tolerate internal substitutions, but the protein dynamics apparently are affected, as reflected in rates of hydride transfer. The A317C substitution is not solely responsible for the larger kinetic constants in human ADH4; thus, the differences in catalytic activity must arise from one or more of the other hundred substitutions in the enzyme.

Keywords

Alcohol dehydrogenase; Mutagenesis; X-ray crystallography; Kinetics; Simulation

[*]Corresponding author. Tel.: +1 319-335-7909; fax: +1 319-335-9570. bv-plapp@uiowa.edu.
[1]Current address: Department of Biochemistry and Molecular Biology, Iowa State University, Ames, Iowa, USA.

Conflicts of Interest
None

1. Introduction

Kinetic constants, including K_m values, binding constants and turnover numbers, for enzymes are determined by protein structure, but quantitative explanations are challenging even when high resolution structures of the enzyme-substrate complexes are available. Sometimes predictions based on examination of structures qualitatively fit the results of site-directed mutagenesis, but magnitudes of the effects vary. For instance, substitution with an arginine residue for a histidine residue that interacts with the pyrophosphate of the coenzyme in yeast and human alcohol dehydrogenases can increase affinity for coenzymes over a range of 2–50-fold [1–4]. Of course, the binding constants arise from the cooperative effects of many amino acid residues that participate in binding. Furthermore, amino acid residues that are distant from the active site may affect binding through dynamic effects, such as altering conformational changes, and thereby affect several kinetic constants [5–6]. For the Ordered Bi Bi mechanism of ADH, release of the product coenzyme is typically rate-limiting for turnover, so that changes in protein structure that increase dissociation constants of coenzymes can increase activity [7].

The objective of this work is to explain what structural features contribute to the relatively high activity of human alcohol dehydrogenase 4 ("stomach" or σ, coded by gene *ADH7* [8]). The kinetic constants of ADH4 are substantially larger (10–100-fold) than those for human class I and horse liver alcohol dehydrogenases [2,9–15]. The different kinetic constants are probably relevant for the different metabolic roles of the enzymes [16–19]. The amino acid sequences of human ADH4 and the other class I human enzymes are about 69% identical [8,19], and the three-dimensional structures are very similar [10]. The X-ray structures of the human ADH1B*1 and human ADH4 superimpose with a root mean square distance of 0.60 Å for alpha carbon atoms if residues 113–130 and 244–262 (due to deletion of 117 in ADH4 and substitution of glycine residues 260 and 261 in ADH1B*1 with asparagine residues in ADH4) are excluded. Most of the amino acid residues involved in coenzyme binding are the same in the two ADHs, but several residues differ in the substrate binding site, contributing to differences in substrate specificity. A significant change is at residue 317, which is Ala in class I enzymes and Cys in ADH4, and it was suggested that this substitution may account for differences in catalytic efficiency [10]. As shown in Fig. 1, residue 317 contributes its backbone carbonyl oxygen to form a hydrogen bond with the nicotinamide amide nitrogen of the coenzyme, and local changes in structure result in a twist of the nicotinamide ring that could affect binding of coenzyme and hydride transfer. The hypothesis that the A317C substitution increases the kinetic constants was tested by making the substitution in the homologous horse liver alcohol dehydrogenase, E isoenzyme (ADH1E), so that detailed kinetics and high-resolution structures could be compared in a common structural background.

2. Experimental Procedures

2.1 Materials

Materials were purchased from several suppliers: oligodeoxynucleotides used for cloning and mutagenesis from Integrated DNA Technologies; *Pfu* DNA polymerase Turbo from Stratagene; restriction enzymes and T4 DNA ligase from New England Biolabs; isopropyl-β-D-thiogalactopyranoside (IPTG) from Research Products International; DEAE-Sepharose Fast Flow and SP-Sepharose Fast Flow from Amersham Biosciences; pyrazole, 2,3,4,5,6-pentafluorobenzyl alcohol and chloramphenicol from Sigma-Aldrich Chemical Company; ampicillin from Research Products International; nicotinamide adenine dinucleotides ($LiNAD^+$, Na_2NADH) from Roche. Benzyl acohol and benzaldehyde were purchased from Fisher Scientific and redistilled. Bacterial media components were obtained from Becton Dickinson and Company. Plasmid DNA was propagated in *E. coli* DH5α cells (Invitrogen).

Plasmid DNA was purified with kits from Qiagen. DNA fragments were purified using the Qiaquick gel extraction kit (Qiagen). The pET 23d(+) plasmid used for sub-cloning and the *E. coli* BL21 (λDE3) Rosetta cells were obtained from Novagen.

2.2 Plasmid Construction and Mutagenesis

The open reading frame encoding wild-type horse liver alcohol dehydrogenase in the plasmid pBPE [20] was sub-cloned into the expression plasmid pET23d(+) using standard molecular biology techniques. Briefly, the gene was amplified by polymerase chain reaction using primers complementary to the 5′ and 3′ region of the gene. The forward primer (5′-GGAAACAGACC*ATG*GGCACAGCAGGAAAAG-3′) encoded an *Nco*I site (underlined) harboring the ATG start codon (italicized); the reverse primer (5′-GCAGACATTTGTCTCG*AGT*CAAAACGTCAGGATGG-3′) encoded a *Xho*I site (underlined) downstream of the stop codon (italicized). The amplified cDNA and pET23d(+) plasmid were digested with the *Nco*I and *Xho*I restriction enzymes, and the fragments were purified on an agarose gel and ligated overnight at 4 °C. The integrity of the gene was verified by DNA sequence analysis. As a result of the *Nco*I digestion, Ser-1 would be substituted with Gly in the protein. Therefore, the wild-type vector was mutated back to a Ser prior to further mutagenesis using the primers described below.

The Stratagene QuikChange site-directed mutagenesis protocol was used to generate the desired mutations, which were confirmed by DNA sequencing of the coding region by The University of Iowa DNA Facility. The following primers (mutated bases in italics) were used: A317C substitution, 5′-GGACGTACCTGGAAAGGA*TGT*ATTTTTGGCGG-3′ and 5′-CCGCCAAAAAT*ACA*TCCTTTCCAGGTACGTCC-3′; G1S substitution, 5′-GGAGATATACCATG*AGC*ACAGCAGGAAAAG-3′ and 5′-CTTTTCCTGCTGT*GCT*CATGGTATATCTCC-3′.

2.3 Enzyme Expression and Purification

Chemically competent *E. coli* BL21(λDE3) Rosetta cells were transformed with the newly constructed vector and spread onto LB agar plates containing 100 μg/ml ampicillin (amp) and 34 μg/ml chloramphenicol (cam). These plates were incubated overnight at 37 °C. A single colony was used to inoculate 2 ml of LB-amp-cam medium and the culture was allowed to grow to moderate turbidity ($O.D._{600}$ ~0.3). This culture (0.1 ml/plate) was used to inoculate 20 LB-amp-cam agar plates. The plates were incubated overnight at 37 °C. The resulting lawns were used to inoculate 1 l LB-amp-cam medium. The liquid culture was incubated at 28 °C for 1 hr and expression of ADH was induced with 1 mM IPTG. The cells were harvested by centrifugation 18–20 hr after induction. About 15 g of wet cells was obtained, and the enzyme was purified by the published procedure [20]. The protein concentration was determined spectrophotometrically using an extinction coefficient (ε_{280} = 0.455 $cm^{-1}mg^{-1}ml$). The concentration of active sites of enzyme (N) was determined by titration with NAD^+ in the presence of pyrazole [21].

2.4. Steady-State Kinetics

Initial velocities for the change of NADH concentration were determined fluorometrically using an excitation wavelength of 340 nm and monitoring the emission at 460 nm using a FluoroLog SPEX 3-21. All assays were done at 25 °C in the presence of 33 mM sodium phosphate, 0.25 mM EDTA, buffer, pH 8.0, and started with the addition of enzyme. Initial velocities were calculated by fitting the curves either with a linear or parabolic function. Data for the forward reaction obtained with varied concentrations (5 concentrations over a nine-fold range) of both NAD^+ and benzyl alcohol showed an intersecting initial velocity pattern and were fitted to the equation for a sequential bi mechanism with the program SEQUEN [22], which gave good estimates of the Michaelis constants for NAD^+ and benzyl

alcohol, the dissociation constant for NAD^+ (K_{ia}), and V_1. Similar data for the reverse reaction with NADH and benzaldehyde showed a parallel initial velocity pattern and gave a poor fit for the dissociation constant for NADH (K_{iq}) when fitted with the program SEQUEN, and therefore these data were fitted with the program PINGPONG [22], which provided the true Michaelis constants for benzaldehyde and NADH and V_2. (The kinetic mechanism for ADH1E has been established to be Ordered Bi Bi, but since the commitment factors favor the reaction of NADH and benzaldehyde, the initial velocity pattern can appear to be ping pong.) Product inhibition studies were used to determine the inhibition (dissociation) constants for NAD^+ or NADH by varying the concentration of one coenzyme over a range from 0.3–2.5 times the K_m, fixing the substrate concentration at near saturation, and varying the concentration of the inhibitor coenzyme over a range from 0–5 times the K_i value. These data were fitted to the equation for competitive inhibition (COMP [22]).

2.5. Transient Kinetics

A Bio-Logic SFM-3 stopped-flow instrument with a path length of 1.0 cm and a dead time of 2.5 ms was used to obtain transient data. All reactions were studied at 25 °C in 33 mM sodium phosphate and 0.25 mM EDTA buffer, pH 8.0.

The rate constant for binding of NAD^+ was determined by trapping the enzyme-NAD^+ complex with pyrazole [23,24]. Enzyme (15 μN final concentration) was allowed to react with varied concentrations of NAD^+ (32–238 μM) and 10 mM pyrazole, and the change in absorbance at 293 nm was monitored for the formation of the E-NAD^+-pyrazole complex. The progress curves were fitted using the Bio-Kine software to an exponential function to determine the observed first-order rate constant. From the dependence of k_{obs} on NAD^+ concentration, the second-order rate constant for binding of NAD^+ was calculated.

Binding of NADH to the enzyme was measured by the quenching of intrinsic protein fluorescence in the enzyme-NADH complex [25,26]. Enzyme (2.1 μN) was allowed to react with varied concentrations of NADH, and the reaction was followed by the fluorescence emission between 315–384 nm with excitation at 297 nm. Values for microscopic rate constants for the simple binding mechanism, E + NADH = E-NADH, were estimated by simulation of the full progress curves using KINSIM/FITSIM [27].

The transient reactions of coenzyme and substrate were studied with 14 μN enzyme, fixed concentration of coenzyme (1 mM NAD^+ or 64 μM NADH) and varied concentrations of benzyl alcohol or benzaldehyde. The reactions were monitored by the change in absorbance of NADH at 328 nm where the free and enzyme-bound forms of NADH have the same extinction coefficient (isosbestic point) of $\varepsilon = 5.5\ mM^{-1}cm^{-1}$ [28]. The microscopic rate constants for a complete Ordered Bi Bi mechanism were estimated by using KINSIM/FITSIM to fit the progress curves for the forward and reverse reactions, with the rate constants for coenzyme binding fixed as determined independently.

2.6. X-ray crystallography

The A317C alcohol dehydrogenase (0.7 ml, 11 mg/ml) was dialyzed (five exchanges) against 10 ml ammonium *N*-[tris(hydroxymethyl)methyl]-2-aminoethanesulfonate buffer (pH 7.0, 4 °C), 0.25 mM EDTA, and on the fifth exchange, the dialysis buffer also contained 5 mM 2,3,4,5,6-pentafluorobenzyl alcohol and 11 mM $LiNAD^+$. Crystals formed after the slow, cumulative addition of 100% 2-methyl-2,4-pentanediol (MPD) to about 14% MPD, and the final concentration of MPD was brought to 25%. The resulting crystals were mounted on fiber loops and flash cooled at 100 °K by immersion into liquid N_2. X-ray data were collected at 100 K using beam line 4.2.2 at the Advanced Light Source at Berkeley with X-rays at 0.80 Å, at 97 mm distance with 0.5 deg oscillations over 360 degrees. Data

were processed with d*TREK [29]. Structures were solved by molecular replacement with the coordinates for the refined complex of wild-type ADH complexed with NAD^+ and 2,3,4,5,6-pentafluorobenzyl alcohol (1HLD.pdb, [30]). The initial model for the A317C enzyme had Ala-317. The structure was refined by cycles of restrained refinement with REFMAC [31] and model building with the program O [32] and checked with PROCHECK [33].

3. Results and Discussion

3.1. Kinetic characterization

The steady-state kinetics of A317C ADH1E fit the typical Ordered Bi Bi mechanism for ADH1E. Steady-state kinetic constants for the oxidation of benzyl alcohol and the reduction of benzaldehyde catalyzed by the A317C enzyme were comparable to those for the recombinant wild-type horse E enzyme (Table 1). The largest differences were a 1.8-fold decrease in the Michaelis constant for benzyl alcohol, about 1.7-fold increases in the dissociation constants for the NAD^+ and NADH, and a 2.3-fold increase in the catalytic efficiency for the oxidation of benzyl alcohol. Although these changes are small, they appear to be significant. However, as shown in Table 1, the kinetic constants for human ADH4 are 15–40-fold higher than those for horse ADH1E, and the A317C substitution at Ala-317 does not increase the kinetic constants to such a level. As an illustration that substitutions in horse ADH1E can affect the kinetic constants, the values obtained for V292S ADH are also presented in Table 1. The V292S substitution indirectly affects coenzyme binding by altering the conformational equilibrium [6].

Since steady-state kinetic constants are macroscopic (ratios of rate constants), transient kinetics data were collected and used to estimate microscopic rate constants for each step in the mechanism (Table 2). The binding of NAD^+ fits a pseudo first order process and was linearly dependent on NAD^+ concentration (data not shown); the rate constant was about 1/2 that of the wild-type enzyme (Table 2). Data to estimate the rate constant for dissociation of the enzyme-NAD^+ complex were not obtained. The binding of NADH was also pseudo first order, but the apparent rate constants and extent of reaction changed as the concentration of NADH was varied, as expected for a reversible equilibrium, allowing rate constants for the forward and reverse reaction to be estimated (Fig. 2). These rate constants were similar to those determined for wild-type enzyme (Table 2).

The remaining rate constants were estimated by using transient kinetic data for the reactions with NAD^+ and benzyl alcohol or NADH and benzaldehyde. (The aromatic substrates are used for this work because they are good substrates and the rate constants for hydride transfer can be measured, and we can compare results with other ADHs.) As shown in Fig. 3, the transient curves have some evidence of a “burst” phase, resulting from rapid hydride transfer followed by slower steps. The estimated rate constant at saturating concentrations of benzyl alcohol was 20 s^{-1}. However, the exponential and steady-state phases are not very well separated, and, in any case, the observed rate constants are complex functions of rate constants for several internal steps. Thus, the family of 8 transient progress curves for the forward and reverse reactions were simulated to provide estimates for the microscopic rate constants (Table 2). For these simulations, the rate constants for binding of coenzyme were fixed at the values determined from the independent transient studies. In such simulations, the progress curves are fitted with non-linear least squares analysis, and the standard errors for each rate constant are estimated. As given in Table 2, the errors are acceptably small, indicating good fits. Nevertheless, these are estimated rate constants, and different concentrations of substrates and different restraints in the simulations can produce somewhat different values, as the “FitSpace” may be large in multidimensional fitting [34]. The rate

constants for hydride transfer for the oxidation of benzyl alcohol and the reduction of benzaldehyde (k_3 and k_{-3}) appeared to decrease by 2.8-fold.

In order to confirm that the hydride transfer step was actually being measured, we determined the progress curves with α,α-d_2-benzyl alcohol, and the transient reactions were considerably slower than with protio benzyl alcohol. Simulations of these reactions, in which all of the rate constants except for step 3 were fixed, showed that the deuterium isotope effect on k_3 was 5.2 ± 1.0, consistent with this step being hydride transfer [7,35]. Thus, the A317C substitution appears to significantly decrease the rate constant for the chemical step. The decrease in k_3 also accounts for the diminished burst phase (Fig. 3) relative to wild-type enzyme since the slowest step, dissociation of NADH (k_5), is comparable in magnitude to k_3 and the transient reaction is controlled by both steps. The decreased rate constant for hydride transfer is also reflected in the steady-state oxidation of benzyl alcohol, as the isotope effects on V_1/E_t and V_1/E_tK_b are 2.2 (data not shown), suggesting that hydride transfer is partially rate-limiting for turnover.

3.2. X-ray crystallography

A317C ADH1E was crystallized with NAD^+ and 2,3,4,5,6-pentafluorobenzyl alcohol, which is an unreactive analogue of the substrate of benzyl alcohol that binds in a mode that resembles the expected Michaelis complex [30]. Data were collected to 1.2 Å resolution at the ALS synchrotron. Table 3 summarizes the data processing and refinement statistics. The overall structure is essentially identical to the structure of the wild-type enzyme, except near residue 317 where the additional sulfhydryl group displaces a water molecule that is present in the wild-type enzyme (Fig. 4). The electron density map for A317C ADH permits the unambiguous placement of the atoms, but there is no density for the water that is hydrogen-bonded to Ser-182 in the wild-type horse or other Class I enzymes. Instead, there is strong density for the sulfhydryl group of Cys-317, which makes a hydrogen bond (3.1 Å) to the hydroxyl group of Ser-182. This interaction does not immobilize the side chain of Ser-182, however, as the hydroxyl group also occupies an alternative position, with 30–35% occupancy (in both subunits of the dimeric enzyme) in which the hydroxyl group of Ser-182 forms a hydrogen bond (2.8 Å) with the carbonyl oxygen of Gly-179. Such an alternative position is not observed in the structure of the wild-type enzyme determined at comparable resolution. In contrast to the structures of human ADH4 as compared to human ADH1B*1 (Fig. 1), the nicotinamide rings of NAD^+ are almost exactly superimposed in the wild-type and A317C horse enzymes, as are all of the other amino acid residues and the pentafluorobenzyl alcohols. There is no significant difference in B factors for the overall protein or the atoms near the A317C substitution for the two horse ADH structures.

Inspection of the structures of the wild-type and A317C horse enzymes provides no obvious explanation for the somewhat different kinetic constants presented in Tables 1 and 2. However, 2–3-fold effects on kinetics are small in terms of the energetics of binding, and the structural changes might be expected to be small. Nevertheless, the 2.8-fold decrease in the rate constants for hydride transfer could be explained by alterations in the enzyme dynamics. Hydrogen is transferred with quantum mechanical tunneling, which is very sensitive to the donor-acceptor distance and protein dynamics [36,37]. Thus, substitutions of amino acid residues that contact the substrate or coenzyme can modulate the apparent degree of tunneling, as was determined with kinetic isotope effects in horse liver ADH [38,39]. Although tunneling is affected by substitutions of various amino acids, the rate constants for hydride transfer may only decrease moderately, for instance, up to 16-fold for the V203A enzyme [35]. It appears that the structure of ADH is relatively stable, but adaptable, and can tolerate substitutions, such as A317C, without greatly affecting catalysis.

It appears that the A317C substitution is not solely responsible for the 10–100-fold increases in kinetic constants for human ADH4 as compared to other class I enzymes. Since human ADH 4 differs at about 115 of 374 residues compared to the other class I enzymes, the differences in kinetics could arise from one or more of the other substitutions. For instance, the Ala-182/Cys-317 pair in ADH4 may alter flexibility as compared to the Ser-182/water/Ala-317 in the class I ADHs (see Fig. 4). Phe-309 is in the substrate (alcohol) binding site of ADH4, but it also makes a close contact with the nicotinamide amide nitrogen, whereas Leu-309 in Class I ADHs is farther away from the amide, and these differences could affect binding of coenzyme. However, the F309L/C317A substitutions made in ADH4 had no effect on binding of NAD^+ while causing large (up to 180-fold) effects on catalytic efficiencies for various aliphatic substrates [10]. The rationale for our experimental design was to examine only one residue that seemed most likely to be responsible for changes in activity, but future studies could examine other amino acid residues at or near the active. Moreover, residues that are more distant from the active site, such as the Gly/Asn substitutions at residues 260 and 261, may also indirectly affect structure and dynamics. Explaining how structure determines the different kinetic constants remains a challenge for ADH and other enzymes.

Acknowledgments

This work was supported by NIH grant GM078446. Data were collected on the Molecular Biology Consortium beamline (4.2.2) at the Advanced Light Source with the assistance of Dr. Jay C. Nix and support from the Office of Science, Office of Basic Energy Sciences of the US Department of Energy under Contract No. DE-AC02-05CH11231.

Abbreviations

ADH alcohol dehydrogenase

References

1. Bosron WF, Magnes LJ, Li TK. Kinetic and electrophoretic properties of native and recombined isoenzymes of human liver alcohol dehydrogenase. Biochemistry. 1983; 22:1852–1857. [PubMed: 6342668]
2. Yin SJ, Bosron WF, Magnes LJ, Li TK. Human liver alcohol dehydrogenase: purification and kinetic characterization of the β2β2, β2β1, αβ2, and β2γ1 “Oriental” isoenzymes. Biochemistry. 1984; 23:5847–5853. [PubMed: 6395883]
3. Hurley TD, Edenberg HJ, Bosron WF. Expression and kinetic characterization of variants of human β1β1 alcohol dehydrogenase containing substitutions at amino acid 47. J Biol Chem. 1990; 265:16366–16372. [PubMed: 2398055]
4. Gould RM, Plapp BV. Substitution of arginine for histidine-47 in the coenzyme binding site of yeast alcohol dehydrogenase I. Biochemistry. 1990; 29:5463–5468. [PubMed: 2201405]
5. Ramaswamy S, Park DH, Plapp BV. Substitutions in a flexible loop of horse liver alcohol dehydrogenase hinder the conformational change and unmask hydrogen transfer. Biochemistry. 1999; 38:13951–13959. [PubMed: 10529241]
6. Rubach JK, Ramaswamy S, Plapp BV. Contributions of valine-292 in the nicotinamide binding site of liver alcohol dehydrogenase and dynamics to catalysis. Biochemistry. 2001; 40:12686–12694. [PubMed: 11601993]
7. Plapp BV. Conformational changes and catalysis by alcohol dehydrogenase. Arch Biochem Biophys. 2010; 493:3–12. [PubMed: 19583966]
8. Satre MA, Žgombić-Knight M, Duester G. The complete structure of human class IV alcohol dehydrogenase (retinol dehydrogenase) determined from the ADH7 gene. J Biol Chem. 1994; 269:15606–15612. [PubMed: 8195208]

9. Kedishvili NY, Bosron WF, Stone CL, Hurley TD, Peggs CF, Thomasson HR, Popov KM, Carr LG, Edenberg HJ, Li TK. Expression and kinetic characterization of recombinant human stomach alcohol dehydrogenase. Active-site amino acid sequence explains substrate specificity compared with liver isozymes. J Biol Chem. 1995; 270:3625–3630. [PubMed: 7876099]
10. Xie P, Parsons SH, Speckhard DC, Bosron WF, Hurley TD. X-ray structure of human class IV σσ alcohol dehydrogenase. Structural basis for substrate specificity. J Biol Chem. 1997; 272:18558–18563. [PubMed: 9228021]
11. Crosas B, Allali-Hassani A, Martínez SE, Martras S, Persson B, Jörnvall H, Parés X, Farrés J. Molecular basis for differential substrate specificity in class IV alcohol dehydrogenases: A conserved function in retinoid metabolism but not in ethanol oxidation. J Biol Chem. 2000; 275:25180–25187. [PubMed: 10829036]
12. Farrés J, Moreno A, Crosas B, Peralba JM, Allali-Hassani A, Hjelmqvist L, Jörnvall H, Parés X. Alcohol dehydrogenase of class IV (σσ-ADH) from human stomach. cDNA sequence and structure/function relationships. Eur J Biochem. 1994; 224:549–557. [PubMed: 7925371]
13. Plapp, BV.; Berst, KB. Human Alcohol Dehydrogenase 4: Mechanism, Specificity and Effects of Ethanol on Retinoid Metabolism. In: Weiner, H.; Plapp, BV.; Lindahl, R.; Maser, E., editors. Enzymology and Molecular Biology of Carbonyl Metabolism 12. Purdue University Press; West Lafayette: 2006. p. 190-199.
14. Charlier HA Jr, Plapp BV. Kinetic cooperativity of human liver alcohol dehydrogenase γ2. J Biol Chem. 2000; 275:11569–11575. [PubMed: 10766771]
15. Dworschack RT, Plapp BV. Kinetics of native and activated isozymes of horse liver alcohol dehydrogenase. Biochemistry. 1977; 16:111–116. [PubMed: 831772]
16. Yin SJ, Wang MF, Liao CS, Chen CM, Wu CW. Identification of a human stomach alcohol dehydrogenase with distinctive kinetic properties. Biochemistry International. 1990; 22:829–835. [PubMed: 2099148]
17. Han CL, Liao CS, Wu CW, Hwong CL, Lee AR, Yin SJ. Contribution to first-pass metabolism of ethanol and inhibition by ethanol for retinol oxidation in human alcohol dehydrogenase family--implications for etiology of fetal alcohol syndrome and alcohol-related diseases. Eur J Biochem. 1998; 254:25–31. [PubMed: 9652389]
18. Algar EM, VandeBerg JL, Holmes RS. A gastric alcohol dehydrogenase in the baboon: purification and properties of a ‘high-Km’ enzyme, consistent with a role in ‘first pass’ alcohol metabolism. Alcohol Clin Exp Res. 1992; 16:922–927. [PubMed: 1443431]
19. Parés X, Cederlund E, Moreno A, Hjelmqvist L, Farrés J, Jörnvall H. Mammalian class IV alcohol dehydrogenase (stomach alcohol dehydrogenase): structure, origin, and correlation with enzymology. Proc Natl Acad Sci USA. 1994; 91:1893–1897. [PubMed: 8127901]
20. Park DH, Plapp BV. Isoenzymes of horse liver alcohol dehydrogenase active on ethanol and steroids. cDNA cloning, expression, and comparison of active sites. J Biol Chem. 1991; 266:13296–13302. [PubMed: 1712777]
21. Theorell H, Yonetani T. Liver Alcohol Dehydrogenase-DPN-Pyrazole Complex: A Model of a Ternary Intermediate in the Enzyme Reaction. Biochem Z. 1963; 338:537–553. [PubMed: 14087322]
22. Cleland WW. Statistical analysis of enzyme kinetic data. Methods Enzymol. 1979; 63:103–138. [PubMed: 502857]
23. Shore JD, Gilleland MJ. Binding and kinetic studies of liver alcohol dehydrogenase-coenzyme-pyrazole complexes. J Biol Chem. 1970; 245:3422–3425. [PubMed: 4318909]
24. LeBrun LA, Plapp BV. Control of coenzyme binding to horse liver alcohol dehydrogenase. Biochemistry. 1999; 38:12387–12393. [PubMed: 10493806]
25. Geraci G, Gibson QH. The reaction of liver alcohol dehydrogenase with reduced diphosphopyridine nucleotide. J Biol Chem. 1967; 242:4275–4278. [PubMed: 4294050]
26. Strömberg P, Svensson S, Berst KB, Plapp BV, Höög JO. Enzymatic mechanism of low-activity mouse alcohol dehydrogenase 2. Biochemistry. 2004; 43:1323–1328. [PubMed: 14756569]
27. Frieden C. Analysis of kinetic data: practical applications of computer simulation and fitting programs. Methods Enzymol. 1994; 240:311–322. [PubMed: 7823836]

28. Theorell H, Bonnichsen R. Studies on Liver Alcohol Dehydrogenase: I. Equilibria and Initial Reaction Velocities. Acta Chem Scand. 1951; 5:1105–1126.
29. Pflugrath JW. The finer things in X-ray diffraction data collection. Acta Crystallogr D Biol Crystallogr. 1999; 55:1718–1725. [PubMed: 10531521]
30. Ramaswamy S, Eklund H, Plapp BV. Structures of horse liver alcohol dehydrogenase complexed with NAD^+ and substituted benzyl alcohols. Biochemistry. 1994; 33:5230–5237. [PubMed: 8172897]
31. Murshudov GN, Vagin AA, Dodson EJ. Refinement of macromolecular structures by the maximum-likelihood method. Acta Crystallogr D Biol Crystallogr. 1997; 53:240–255. [PubMed: 15299926]
32. Jones TA, Zou JY, Cowan SW, Kjeldgaard. Improved methods for building protein models in electron density maps and the location of errors in these models. Acta Crystallogr. 1991; A 47(Pt 2):110–119.
33. Laskowski RA, MacArthur MW, Moss DS, Thornton JM. J Appl Crystallogr. 1993; 26:286–290.
34. Johnson KA, Simpson ZB, Blom T. FitSpace explorer: an algorithm to evaluate multidimensional parameter space in fitting kinetic data. Anal Biochem. 2009; 387:30–41. [PubMed: 19168024]
35. Rubach JK, Plapp BV. Amino acid residues in the nicotinamide binding site contribute to catalysis by horse liver alcohol dehydrogenase. Biochemistry. 2003; 42:2907–2915. [PubMed: 12627956]
36. Klinman JP. Quantum mechanical effects in enzyme-catalysed hydrogen transfer reactions. Trends Biochem Sci. 1989; 14:368–373. [PubMed: 2688201]
37. Nagel ZD, Klinman JP. Tunneling and Dynamics in Enzymatic Hydride Transfer. Chem Rev. 2006; 106:3095–3118. [PubMed: 16895320]
38. Bahnson BJ, Park DH, Kim K, Plapp BV, Klinman JP. Unmasking of hydrogen tunneling in the horse liver alcohol dehydrogenase reaction by site-directed mutagenesis. Biochemistry. 1993; 32:5503–5507. [PubMed: 8504071]
39. Bahnson BJ, Colby TD, Chin JK, Goldstein BM, Klinman JP. A link between protein structure and enzyme catalyzed hydrogen tunneling. Proc Natl Acad Sci USA. 1997; 94:12797–12802. [PubMed: 9371755]
40. Plapp, BV. Catalysis by Alcohol Dehydrogenases. In: Kohen, A.; Limbach, HH., editors. Isotope Effects in Chemistry and Biology. CRC Press; Taylor and Francis, Boca Raton: 2006. p. 811-835.
41. Plapp BV. Enhancement of the activity of horse liver alcohol dehydrogenase by modification of amino groups at the active sites. J Biol Chem. 1970; 245:1727–1735. [PubMed: 4314596]
42. Sekhar VC, Plapp BV. Rate constants for a mechanism including intermediates in the interconversion of ternary complexes by horse liver alcohol dehydrogenase. Biochemistry. 1990; 29:4289–4295. [PubMed: 2161681]
43. Davis GJ, Bosron WF, Stone CL, Owusu-Dekyi K, Hurley TD. X-ray structure of human β3β3 alcohol dehydrogenase. The contribution of ionic interactions to coenzyme binding. J Biol Chem. 1996; 271:17057–17061. [PubMed: 8663387]
44. Xie PT, Hurley TD. Methionine-141 directly influences the binding of 4-methylpyrazole in human σσ alcohol dehydrogenase. Protein Sci. 1999; 8:2639–2644. [PubMed: 10631979]

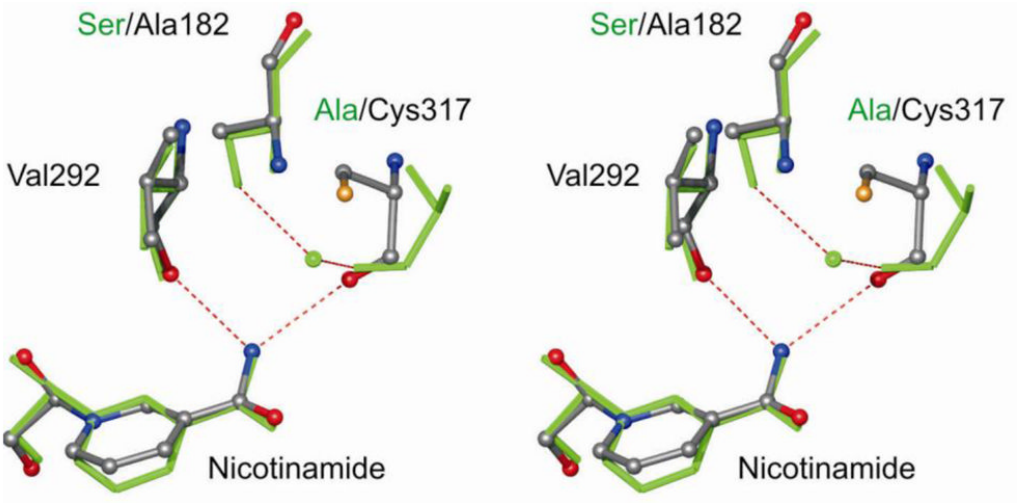

Fig. 1.

Comparison of the structures of human ADH1B*1 and ADH4. In the green, stick representation is ADH1B*1 (1deh.pdb [43]), showing the hydroxyl group of Ser-182 hydrogen bonded to a water molecule, which is also hydrogen bonded to the carbonyl oxygen of Ala-317, and hydrogen bonds from the carbonyl oxygens of Val-292 and Ala-317 to the nicotinamide amide nitrogen of the NAD coenzyme. In atom coloring with spheres is the superposition of ADH4 (1dis.pdb [44]), showing Ala-182 and Cys-317 with its sulfur atom replacing the water in ADH1B*1. The hydrogen bonds to the nicotinamide ring are retained. Note that the nicotinamide rings in the two structures are twisted relative to one another. (The colors are present in the online version.)

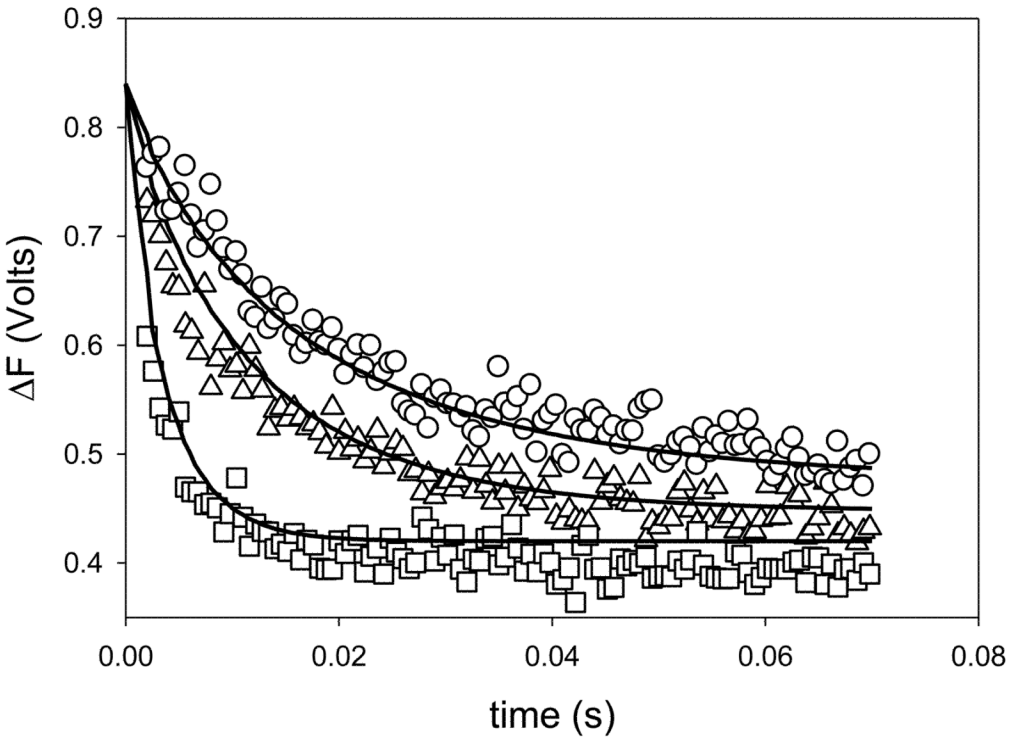

Fig. 2.

Binding of NADH determined by transient kinetics and simulation. Enzyme (2.1 μN) was allowed to react with 3.9 (○), 5.8 (▵) or 17.5 μM (□) NADH. The progress curves were fitted (lines) to the mechanism, E + NADH = E-NADH, where the relative fluorescence of the E-NADH complex was 49 % of that of free E.

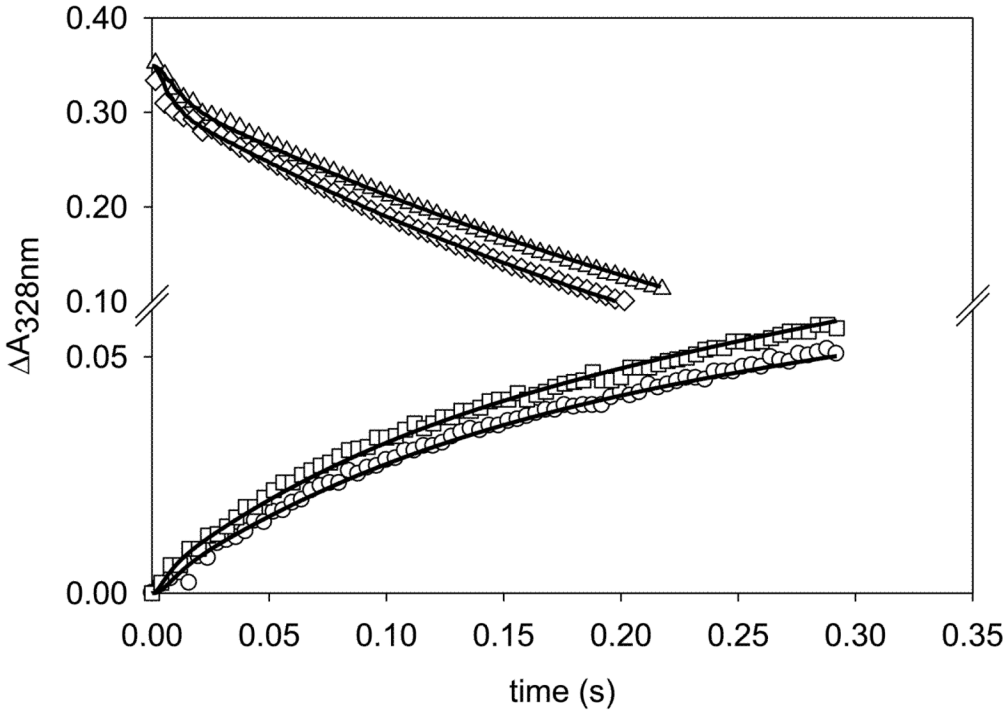

Fig. 3.

Representative progress curves for the transient oxidation of benzyl alcohol and the reduction of benzaldehyde. Enzyme (14.4 μN) was allowed to react with 1 mM NAD^+ and 83 (○) or 500 μM (□) benzyl alcohol or with 64 μM NADH and 160 (▵) or 650 μM benzaldehyde (◊). These progress curves and four additional ones with intermediate concentrations (not shown) were fitted with FITSIM to the mechanism with the rate constants given in Table 2, with an overall *R*-squared value of 0.9998. The lines are the fitted curves.

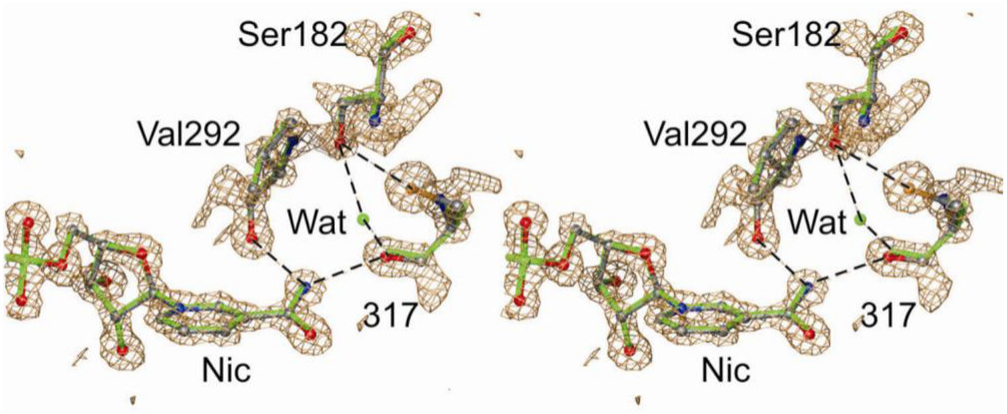

Fig. 4.

Comparison of the structures of wild-type and A317C horse liver alcohol dehydrogenases. In the green, stick representation of wild-type ADH, a water molecule is hydrogen-bonded between the hydroxyl group of Ser-182 and the carbonyl oxygen of Ala-317, and the nicotinamide amide nitrogen is hydrogen bonded to the carbonyl groups of Val-292 and Ala-317 (based on 1hld.pdb [30], data extended to 1.14 Å, unpublished). In atom coloring with spheres is the superposition of A317C ADH with the water molecule displaced by the sulfur atom on Cys-317 and a hydrogen bond between the sulfur of Cys-317 and the hydroxyl group of Ser-182 (this study, 3oq6.pdb). The hydrogen bonds to the nicotinamide ring are present in both structures. Note that the nicotinamide rings in the two structures are in the same positions. The $2|F_o| - |F_c|$ electron density map for A317C ADH is shown. (The colors are shown in the on-line version, and the gray scale figure in the printed version shows that the two structures are almost identical except for the water molecule (no density in the map for A317C ADH) and the sulfur atom of Cys-317 (hydrogen-bonded to Ser-182).

Table 1

Steady-state kinetic constants for recombinant wild-type, A317C and V292S horse liver and recombinant human wild-type class 4 alcohol dehydrogenases acting on benzyl alcohol and benzaldehyde[a].

Kinetic constant	rADH[b]	A317C	V292S[c]	ADH4[d]
K_a (μM)	3.4	5.5	140	140
K_b (μM)	11	6.1	220	230
K_p (μM)	31	23	440	460
K_q (μM)	1.7	2.4	80	51
K_{ia} (μM)	26	41	1600	880
K_{iq} (μM)	0.44	0.71	30	6.0
V_1/E_t (s^{-1})	2.0	2.6	6.3	54
V_2/E_t (s^{-1})	21	21	160	660
$V_1/E_t K_b$ ($mM^{-1}s^{-1}$)	180	420	28	240
$V_2/E_t K_p$ ($mM^{-1}s^{-1}$)	680	900	360	1400
K_{eq} (pM)[e]	45	80	32	57
Turnover number (s^{-1})[f]	1.6	1.4	34	31

[a] Kinetic constants were determined at 25 °C in 33 mM sodium phosphate, 0.25 mM EDTA, buffer, pH 8.0. K_a, K_b, K_p, K_q are the Michaelis constants for NAD^+, benzyl alcohol, benzaldehyde, and NADH, respectively. K_{ia} and K_{iq} are the inhibition constants for NAD^+ and NADH, respectively. V_1/E_t is the turnover number for benzyl alcohol oxidation, and V_2/E_t is the turnover number for benzaldehyde reduction. The standard error of the fits were generally < 15% of the values.

[b] Recombinant wild-type enzyme data from [40].

[c] Data from [6].

[d] Human ADH4 data from [13] determined at 37 °C in 83 mM potassium phosphate, 40 mM KCl and 0.25 mM EDTA buffer, pH 7.3.

[e] K_{eq} is the Haldane relationship calculated from $V_1K_pK_{iq}[H^+]/V_2K_bK_{ia}$. Directly estimated values range from 35–70 pM.

[f] Turnover number determined in a standard enzyme assay at 25 °C [41] based on titration of active sites.

Table 2

Estimated rate constants for the oxidation of benzyl alcohol and reduction of benzaldehyde by wild-type and A317C alcohol dehydrogenases by the Ordered Bi Bi mechanism[a].

$$E \underset{k_{-1}}{\overset{k_1}{\rightleftharpoons}} E\text{-}NAD^+ \underset{k_{-2}}{\overset{k_2}{\rightleftharpoons}} E\text{-}NAD^+ - RCH_2OH \underset{k_{-3}}{\overset{k_3}{\rightleftharpoons}} E\text{-}NADH\text{-}RCHO \underset{k_{-4}}{\overset{k_4}{\rightleftharpoons}} E\text{-}NADH \underset{k_{-5}}{\overset{k_5}{\rightleftharpoons}} E$$

rate constant	wild-type ADH[b]	A317C ADH
k_1 ($M^{-1}s^{-1}$)	1.2 (± 0.12) × 10^6	5.9 (± 0.25) × 10^5[c]
k_{-1} (s^{-1})	56 ± 6	72 ± 4
k_2 ($M^{-1}s^{-1}$)	3.7 (± 0.37) × 10^6	2.8 (± 0.75) × 10^6
k_{-2} (s^{-1})	58 ± 5	43 ± 2
k_3 (s^{-1})	38 ± 3	14 ± 0.4
k_{-3} (s^{-1})	310 ± 30	106 ± 2
k_4 (s^{-1})	66 ± 6	68 ± 3
k_{-4} ($M^{-1}s^{-1}$)	8.3 (± 0.83) × 10^5	1.1 (± 0.26) × 10^6
k_5 (s^{-1})	5.5 ± 0.5	4.4 ± 0.2 (5.9 ± 0.2)[d]
k_{-5} ($M^{-1}s^{-1}$)	1.1 (± 0.11) × 10^7	1.5 (± 0.12) × 10^7[c]

[a] Determined from the simulation and fitting of the progress curves for the transient oxidation of benzyl alcohol and the reduction of the benzaldehyde at pH 8 and 25 °C. The data were fitted to the mechanism shown. Eight progress curves, four forward and four reverse reactions (some shown in Fig. 3) were used for the simulation.

[b] Data from [42].

[c] The rate constants for coenzyme binding were determined independently and fixed in the simulation.

[d] Rate constant determined independently as shown in Fig. 2.

Table 3

X-ray data and refinement statistics for A317C horse liver alcohol dehydrogenase complexed with NAD^+ and 2,3,4,5,6-pentafluorobenzyl alcohol.

PDB entry	3OQ6
space group	P_1
cell dimensions, Å	44.34, 51.31, 92.21
cell angles, deg	91.98, 102.95, 110.11
no. of dimeric molecules per unit cell	1
resolution range, Å	20.0–1.20
no. of observed reflections	765672
no. of unique reflections	214172
completeness, % (outer shell)	92.2 (83.6)
R_{merge}, % (outer shell)[a]	6.1 (28.1)
mean$\langle I\rangle/\sigma\langle I\rangle$(outer shell)	9.4 (3.0)
R_{value}, R_{free}, test %[b]	0.135, 0.162, 0.5
rmsd for bond distances, Å[c]	0.014
rmsd for bond angles, deg[c]	1.62
estd errors in coordinates, Å	0.026
no. of water molecules	1098

[a] $R_{merge} = (\Sigma|I - \langle I\rangle|)/\Sigma\langle I\rangle$, where I is the integrated intensities of a given reflection.

[b] $R_{value} = (\Sigma|F_O - kF_C|)/\Sigma|F_O|$, where k is a scale factor. The R_{free} value was calculated with the indicated percentage of reflections not used in the refinement.

[c] Root-mean-square deviations (rmsd) from ideal geometry of the final model.